Pergamon

Pattern Recognition, Vol. 30, No. 7, pp. 1183–1189, 1997

0031-3203/97 $17.00+.00

PII: S0031-3203(96)00145-8

AN ADAPTIVE IMAGE ENHANCEMENT ALGORITHM

JORGE A. SILVA CENTENO[†] and VICTOR HAERTEL[†*]

[†]Institut für Photogrammetrie und Fernerkundung, Universität Karlsruhe, D-76128 Karlsruhe, Germany
[‡]Remote Sensing Center, Federal University of Rio Grande do Sul Caixa Postal 15044, Porto Alegre 91501-790, Brazil

(*Received* 21 *March* 1996; *in revised form* 8 *August* 1996; *received for publication* 17 *September* 1996)

Abstract—Image enhancement is a common procedure intended to process an image so that the resulting processed image is more suitable than the original one for a given application. Spatial filtering is a well-known procedure to achieve this goal. Low-pass filtering smooths the image and is often used as a preprocessing step to image analysis, removing small details and reducing noise. This filtering process, however, blurs the image. High-pass filtering sharpens the borders between the different image regions by highlighting edges. This process also highlights noise and spurious details. This study proposes a different method that first detects borders between radiometrically distinct image regions and then applies a weighting function to smooth each region internally. The proposed algorithm was implemented on a SUN Sparcstation for testing purposes. Results of the procedure are presented. © 1997 Pattern Recognition Society. Published by Elsevier Science Ltd.

Image enhancement | Remote sensing | Edge detection | Image filtering
Image segmentation | Test of hypothesis

1. INTRODUCTION

Image enhancement techniques are useful tools to process an image so that the resulting image is more adequate for some specific application. It presents a wide range of applications in image analysis. Several well-known techniques have been proposed and are extensively discussed in the literature. For a general review, the reader is referred to Gonzalez and Woods,[1] Rosenfeld and Kak,[2] among others. The actual method to be used in image enhancement depends on the specific application the analyst has in mind. A method that is useful for one particular problem may turn out to be inadequate when dealing with a different application, i.e. it depends on the specific application.

Image enhancement techniques can be grouped into two broad categories: (1) enhancement by point processing and (2) enhancement by spatial filtering. The first category comprises methods that are based only on the brightness of single pixels, whereas methods in the second category are characterized by operations over neighborhoods. Techniques involving histogram modification are point processing methods. Spatial filtering is a neighborhood method, and is widely applied to remote sensing imagery for both image smoothing and sharpening. Spatial filtering can be performed either in the spatial domain or in the frequency (or Fourier) domain. In the spatial domain, spatial filtering is implemented by using spatial masks, also known as "moving windows". Low-pass filters attenuate or eliminate high-frequency components in the Fourier domain while leaving low frequencies untouched. This results in image smoothing or blurring. Similarly, high-pass filters attenuate or eliminate low frequencies, sharpening the edges and other transitions, including image noise.

In remote sensing imagery, both filters are extensively used. A common application of low-pass filters is noise attenuation or removal. It is also frequently used as an image preprocessing step to remove small variations within image regions. A drawback in low-pass filtering is the general blurring that results, specially along the borders between the radiometrically distinct image regions. High-pass filtering is a tool to sharpen the borders between these regions, making it easier to identify the different image regions. A drawback in high-pass filtering lies in the fact that this procedure increases the within-region radiometric variations and also image noise.

The method proposed in this study aims to smooth the radiometrically uniform areas across an image and, at the same time, sharpen the borders between them. To some extent it combines the advantages of both low-pass and high-pass filtering, minimizing the drawbacks which are inherent to each procedure when applied individually.

2. METHODOLOGY

The image enhancement technique, as proposed in this study, involves two distinct steps: (1) detection of the edges or boundaries between image regions, and (2) assigning to each pixel a new digital number (DN), more representative of the region which it belongs to. This procedure should accomplish the goal of improving the

* Author to whom correspondence should be addressed. E-mail: haertel@if1.if.ufrgs.br.

overall image visual perception by sharpening the boundaries between classes and, at the same, time smoothing the internal tonal variations across each region or image class. The internal tonal diversity across many individual classes is due to local variations or simply noise and, for many applications, is not significant in the analysis procedure but may rather hamper it.

Following this approach, the initial problem to be dealt with is the segmentation of the image into more or less homogeneous regions. Once the segmentation procedure has been accomplished, the image will be enhanced by applying to the segmented regions an enhancing function that will assign to each pixel an appropriate DN.

2.1. *Image segmentation*

Since we have no prior knowledge of the region boundaries across the image, the segmentation process as well as the implementation of the enhancing function are performed across small areas at a time. The concept of moving window can be used to perform this task.

A digital image can be described by a function:

$$z = f(x, y)$$

where x is the pixel row number, y is the pixel column number and z is the DN associated with the pixel.

In an ideal image, z is constant within each class described by a radiometrically homogeneous region. In this case, z represents the DN associated with this particular class.

An ideal image can thus be represented by a set of horizontal planes, with sharp boundaries between them. Given a small sub-region, a plane can be fitted to the digital numbers. If the sub-region is entirely contained in a single class, i.e. is an homogeneous region, then the plane will be zero-sloped, whereas if a border is present, then a sloped plane will result. This approach provides a decision rule about the homogeneity of the image region under consideration. This basic idea was proposed by Haralick[3] in edge detection and is used in this study.

In real images, no region is perfectly homogeneous, i.e. with constant DN. Rather, a region (representing one particular image class) can be described by a flat surface with noise superimposed on it. In general,

$$f(x, y) = a1 * x + a2 * y + a3 + e(x, y), \qquad (1)$$

with $e(x, y) \sim N(0, \sigma^2)$, i.e. the noise is normally distributed with mean equal to zero and variance σ^2. It is also assumed that the noise associated with any two pixels is independent.

The standard least-squares procedure can be used to estimate the parameters $a1$, $a2$, and $a3$, i.e. $\hat{a}1$, $\hat{a}2$, and $\hat{a}3$, which minimize the summation of the squares of the residuals at each pixel within the region:

$$S^2 = \sum_x \sum_y [\hat{a}1 * x + \hat{a}2 * y + \hat{a}3 - f(x, y)]^2. \qquad (2)$$

In order to estimate S^2, we have to improve the definition of the coordinate system (x,y). As shown by Haralick,[3] it turns out that the computations are much simpler if we take a region (moving window) symmetric with respect to the central pixel, i.e. with an odd number of rows and columns and the origin at the central pixel (0,0). Following this conventional procedure, we obtain:

$$\hat{a}1 = \frac{\sum_x \sum_y x * f(x, y)}{\sum_x \sum_y x^2}, \qquad \hat{a}2 = \frac{\sum_x \sum_y y * f(x, y)}{\sum_x \sum_y y^2},$$
$$\hat{a}3 = \frac{\sum_x \sum_y f(x, y)}{\sum_x \sum_y 1}. \qquad (3)$$

Recalling that:

$$f(x, y) = a1 * x + a2 * y + a3 + e(x, y),$$

we obtain, for this particular coordinate system:

$$\hat{a}1 = a1 + \frac{\sum_x \sum_y x * e(x, y)}{\sum_x \sum_y x^2},$$
$$\hat{a}2 = a2 + \frac{\sum_x \sum_y y * e(x, y)}{\sum_x \sum_y y^2},$$
$$\hat{a}3 = a3 + \frac{\sum_x \sum_y e(x, y)}{\sum_x \sum_y 1}. \qquad (4)$$

Applying the law of propagation for variances and covariances we obtain:

$$\sigma^2_{\hat{a}1} = \frac{\sigma^2}{\sum_x \sum_y x^2}, \sigma^2_{\hat{a}2} = \frac{\sigma^2}{\sum_x \sum_y y^2}, \sigma^2_{\hat{a}3} = \frac{\sigma^2}{\sum_x \sum_y 1}. \qquad (5)$$

Also, from equation (4), it can be easily shown that since $e(x,y)$ is independent across the image, we have,

$$\sigma_{\hat{a}1,\hat{a}2} = \sigma_{\hat{a}1,\hat{a}3} = \sigma_{\hat{a}2,\hat{a}3} = 0,$$

i.e. $\hat{a}1$, $\hat{a}2$, and $\hat{a}3$ are independent. From equations (1), (2) and (4), it can be shown that:

$$S^2 = \sum_x \sum_y e^2(x, y) - (\hat{a}1 - a1)^2 \sum_x \sum_y x^2 - (\hat{a}2 - a2)^2 \sum_x \sum_y y^2 - (\hat{a}3 - a3)^2 \sum_x \sum_y 1. \qquad (6)$$

Also, since $e(x, y) \sim N(0, \sigma^2)$, it follows that:

$$\frac{\sum_x \sum_y e^2(x, y)}{\sigma^2} \sim X^2_n, \qquad (7)$$

where X^2_n stands for the chi-squared distribution with n degrees of freedom, n being computed by

$$n = \sum_x \sum_y 1.$$

It is assumed that $e(x,y)$ is normally distributed. Thus, $f(x,y)$ being a linear function of $e(x,y)$ is also normally distributed. For the same reason $\hat{a}1$, $\hat{a}2$, and $\hat{a}3$ in equation (4) follow the normal distribution:

$$\hat{a}1 \sim N(a1, \sigma^2_{\hat{a}1}),\ \hat{a}2 \sim N(a2, \sigma^2_{\hat{a}2}),\ \hat{a}3 \sim N(a3, \sigma^2_{\hat{a}3}), \qquad (8)$$

with the variances given in equation (5), it follows that:

$$\frac{(\hat{a}1 - a1)^2}{\sigma^2_{\hat{a}1}} = \frac{(\hat{a}1 - a1)^2 \sum_x \sum_y x^2}{\sigma^2} \sim X^2_1,$$
$$\frac{(\hat{a}2 - a2)^2}{\sigma^2_{\hat{a}2}} = \frac{(\hat{a}2 - a2)^2 \sum_x \sum_y y^2}{\sigma^2} \sim X^2_1,$$
$$\frac{(\hat{a}3 - a3)^2}{\sigma^2_{\hat{a}3}} = \frac{(\hat{a}3 - a3)^2 \sum_x \sum_y 1}{\sigma^2} \sim X^2_1. \quad (9)$$

Then, from equations (6), (7) and (9) it follows that,

$$\frac{S^2}{\sigma^2} \sim X^2_{(n-3)}. \quad (10)$$

Recall that, given two random variables

$$U \sim X^2_j, \qquad V \sim X^2_k,$$

we have

$$\frac{U/j}{V/k} \sim F_{j,k}.$$

From equations (9) and (10) we obtain:

$$\frac{[(\hat{a}1 - a1)^2 \sum_x \sum_y x^2 + (\hat{a}2 - a2)^2 \sum_x \sum_y y^2]/2}{S^2/(n-3)} \sim F_{(2,n-3)}. \quad (11)$$

These statistics can be used to test the following hypotheses:

H_0: The image region is homogeneous, i.e. $a1=0$ and $a2=0$.

against

H_1: The image region is not homogeneous, i.e. $a1 \neq 0$ and/or $a2 \neq 0$.

This simple test of hypothesis can then be used to decide whether the window in a particular position contains one or two classes. By moving the window across the image, the entire image can be segmented into spectrally uniform regions.

2.2. *The image enhancement procedure*

The sharpening procedure, as proposed in this paper, is accomplished by assigning new values to the digital numbers across the entire image, which can be considered more representative of the class to which they belong. This procedure allows the internal smoothing of the classes present on the image and at the same time, the sharpening of the borders between classes. The overall procedure results in a sharper image, more appropriate to visual analysis, and is implemented by a weighting function.

In order to define the proposed weighting function, it is first necessary to define a reference value (RV) for the digital number within the window. Here the outcome of the test of hypothesis is taken into account.

If only one class is present, then the reference value is taken as the average over the digital numbers within the window, rounded to the nearest integer.

If two classes are present, then the reference value is taken as the highest or the lowest digital number within the window, the one closest to the digital number of the central pixel:

```
d1 = DN(central pixel) − DNmin(window)
d2 = DNmax(window) − DN(central pixel)
if (d1 > d2)
   RV = DNmax(window)
else
RV = DNmin(window)
```
(12)

A simple approach, similar to the one proposed by Kramer and Bruckner,[4] consists of simply replacing the central pixel's digital number by the reference value. This procedure, however, does not take into consideration the radiometric characteristics of the region within the window. That means that neighborhoods that generated values close to the threshold adopted for the F-test (Section 2.1), i.e. somehow ambiguous cases, are treated in the same manner as homogenous regions or well-defined edges.

To overcome this problem, we introduce a weighting function, which is meant to control the degree to which the central pixel's digital number approaches the reference value:

$$\mathrm{DN(new)} = \mathrm{WF} * \mathrm{RV} - (1 - \mathrm{WF}) * \mathrm{DN(old)}, \quad (13)$$

with DN(old) being the digital number at the central pixel (original image), DN(new) being the digital number at the central pixel (enhanced image), and WF being the weighting factor.

In this study the weighting function equation (13) is implemented to the central pixel in the window and takes into consideration (i) the existing contrast across the entire image, (ii) the contrast within the window, and (iii) the digital number at the central pixel. Of paramount importance in equation (13) is the estimation of the weighting factor (WF). In this study WF is estimated in two different ways (WF1 and WF2):

Initially, the relative contrast within the window (WCON) is estimated by

$$\mathrm{WCON} = \frac{\mathrm{DNmax(window)} - \mathrm{DNmin(window)}}{\mathrm{DNmax(image)} - \mathrm{DNmin(image)}},$$

with DNmax being highest digital number (across the window or the image), and DNmin being lowest digital number (across the window or the image).

One possible way (WF1) of estimating the weighting factor, according to the test of hypothesis as proposed in Section 2.1, is:

If only one class is present within the window, then

$$\mathrm{WF1} = 1 - \mathrm{WCON}.$$

If two classes are present within the window, then

$$\mathrm{WF1} = \mathrm{WCON}.$$

This weighting factor serves as a measure of the radiometric characteristics across the window, relative to the entire image. If two classes are present, then WF1

can be used as a measure of the radiometric difference between both classes. WF1 close to 1 implies large radiometric contrast, whereas WF1 close to zero means a low contrast between the two classes. If the window contains a single class, then WF1 serves as a measure of the class radiometric homogeneity. WF1 close to 1 implies a nearly radiometrically uniform class, whereas a value close to zero shows large variations within the class.

This approach to the weighting factor, however, does not work well when the two classes as detected by the test of hypotheses are radiometrically close to each other. In this case, the radiometric distance of the central pixel to the reference value (12) can be used. If the digital number at the central pixel is "close" to the reference value, then it is reasonable to introduce a larger change in it, in order to approach it to the reference value. If the digital number is "far" from the reference value, then a large change may introduce error. In this case, a small change is advisable. Therefore, a second possibility (WF2) of estimating the weighting factor is

$$\mathrm{WF2} = 1 - \frac{abs\,[\mathrm{RV} - \mathrm{DN(central\ pixel)}]}{\mathrm{WCON}}.$$

Both weighting factors can be seen as fuzzy functions, which describe the degree to which the neighborhood is well defined as having one or two classes. Here we use the fuzzy logic combination rule of union to derive a new function. As in Pal and Dutta Mahunder,[5] if "C" is the union of two sets "A" and "B", then "C" is described by

$$\mathrm{C} = \vee(\mathrm{A}, \mathrm{B}) = \max(A, B).$$

Using this approach, the WF can be estimated by:

$$\mathrm{WF} = \max(WF1, WF2).$$

WF should assume high values when there are "clearly" defined edges or homogeneous neighborhoods but lower values in ambiguous situations, preserving the original information.

The meaning of the weighting function (13) is clear. It tends to smooth the radiometric differences within class and increase the differences between classes, resulting in an overall sharpening of the image.

3. EXPERIMENTS

The proposed algorithm was tested in two different images: the well-known Lenna image [Fig. 1(a)] and a satellite image (LANDSAT) displaying agricultural fields and some clouds [Fig. 2(a)]. The Lenna image presents several edges and areas with varying gray levels which can be used to test the proposed algorithm. The LANDSAT image is even more adequate for testing the algorithm. The presence of clouds and their shadows with poorly defined edges along with agricultural fields provide the ideal conditions to test the algorithm, which is meant to sharpen the edges and remove noise from more or less homogeneous areas.

The algorithm was implemented using a 3×3 moving window. Figures 1(b) and 2(b) show the results of the F-

(a) (b) (c) (d)

Fig. 1. (a) Lenna Image. (b) Lenna image: results of the F-test (level of significance = 10%). (c) Enhanced Lenna image (one iteration). (d) Enhanced Lenna image (four iterations).

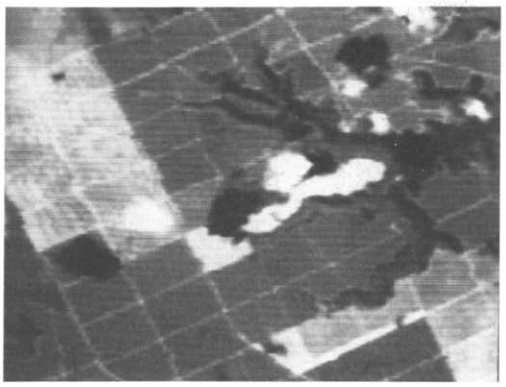

(a)

(b)

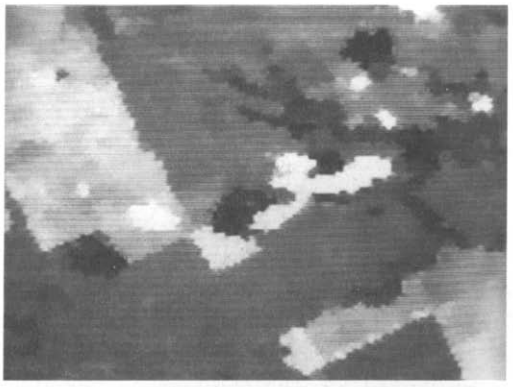

(c)

Fig. 2. (a) Landsat image. (b) Landsat image: results of the F-test (level of significance = 10%). (c) Enhanced Landsat image (four iterations).

test (level of significance of 10%) in images in Figures 1(a) and 2(a), respectively. In these two figures, a dark gray level means that the null hypothesis (as in Section 2.1) is accepted (homogeneous region). A light gray level means that the null hypothesis is rejected (edge is present).

Figures 1(c), (d), and 2(c) depict the enhancement procedure applied to images in Fig. 1(a) (one iteration), Fig. 1(a) (four iterations), and Fig. 2(a) (four iterations), respectively.

A visual inspection of Fig. 1(b) shows that the borders or edges were correctly identified. This figure has a general appearance similar to the result of a normal edge detection filter.

Figure 1(c) is the resulting enhanced image after one iteration. Here the homogeneous regions are smoothed, as expected, and the edges are enhanced, giving more contrast to the whole image. Figure 1(d) shows the resulting enhanced image after four iterations. This image appears to possess "flat" regions in terms of digital numbers, and the regions are spatially better defined and separated from each other.

The enhanced LANDSAT image also shows a similar improvement. The fuzzy borders of the clouds and their shadows are clearly defined after four iterations. Also, the agricultural fields appear more regular, with less internal variations as compared with the original image.

In order to allow a closer inspection of the effect of the level of significance set for the F-test, a subset (16×16 pixels) of the Lenna image is presented in numerical form in Fig. 3. Four classes may be easily identified, with digital numbers around 220, 120, 90, and 20. It can be noticed that the borders between the classes are somewhat blurred, due to the presence of mixed pixels.

The effect of the level of significance for the F-test applied to the numerical image in Fig. 3 is illustrated in Figs 4 and 5. In both figures, digit "1" means that the null hypothesis is accepted, i.e. the corresponding pixel lies in an homogeneous area within the window. Digit "2" means that the null hypothesis is rejected, i.e. an edge is present. Figure 4 is computed for a level of significance of 1% and Fig. 5 for a level of 10%.

As expected, the identification of homogeneous regions (or the presence of edges) within the moving window depends on the level of significance adopted for the F-test. Low values for significance reduce the rejection region and, therefore, a larger number of neighborhoods is accepted as homogeneous (no edge). On the other hand, higher values increase the size of the rejec-

LINE \ COLUMN	216	217	218	219	220	221	222	223	224	225	226	227	228	229	230
24	199	211	215	219	219	219	212	195	149	82	87	79	82	85	89
25	191	205	212	216	218	219	218	207	180	119	78	74	84	85	95
26	176	197	208	213	218	220	223	216	201	161	98	80	88	93	87
27	149	187	202	210	216	220	222	223	213	193	141	89	89	88	71
28	117	170	196	208	216	219	220	223	221	209	183	117	91	68	33
29	107	136	181	203	214	218	220	222	224	221	204	158	77	34	16
30	107	112	159	196	207	214	219	222	223	224	217	188	72	17	17
31	108	106	125	176	197	210	216	221	224	227	222	189	46	9	17
32	111	112	115	149	187	207	215	222	226	226	211	124	14	15	17
33	112	113	110	121	164	202	215	223	224	212	165	41	12	17	12
34	113	117	115	115	131	190	210	219	209	170	66	16	16	18	19
35	117	117	120	120	120	162	200	204	167	71	17	16	19	21	17
36	118	116	122	124	123	145	179	142	59	21	18	21	19	19	19
37	121	120	119	126	126	131	111	50	22	19	20	22	16	21	23
38	119	120	122	127	127	107	55	23	20	18	17	20	15	14	19

Fig. 3. Numerical subset of Lenna image.

LINE \ COLUMN	216	217	218	219	220	221	222	223	224	225	226	227	228	229	230
24	2	2	2	2	1	1	2	2	2	2	1	1	2	1	1
25	2	2	2	2	1	1	1	2	2	2	1	1	1	1	1
26	2	2	2	2	2	1	1	2	2	2	2	1	1	1	1
27	2	2	2	2	2	2	1	1	2	2	2	1	1	1	2
28	2	2	2	2	2	2	2	1	1	2	2	2	1	2	2
29	1	2	2	2	2	2	2	1	1	1	2	2	2	2	1
30	1	2	2	2	2	2	2	2	1	1	2	2	2	1	1
31	1	1	2	2	2	2	2	2	2	1	1	2	2	1	1
32	1	1	1	2	2	2	2	2	1	1	1	2	1	1	1
33	1	1	1	2	2	2	2	1	1	1	2	2	1	1	1
34	1	1	1	1	2	2	2	1	1	2	2	1	1	1	1
35	1	1	1	1	1	2	1	1	2	2	1	1	1	1	1
36	1	1	1	1	1	1	1	2	2	1	1	1	1	1	1
37	1	1	2	1	1	1	2	2	1	1	1	1	1	1	1
38	1	1	2	1	1	2	2	1	1	1	1	1	1	1	1

Fig. 4. Results of the F-test (1%).

LINE \ COLUMN	216	217	218	219	220	221	222	223	224	225	226	227	228	229	230
24	2	2	2	2	1	2	2	2	2	2	1	1	2	2	1
25	2	2	2	2	2	1	2	2	2	2	2	1	2	1	1
26	2	2	2	2	2	2	1	2	2	2	2	1	2	1	2
27	2	2	2	2	2	2	1	2	2	2	2	2	1	2	2
28	2	2	2	2	2	2	2	1	2	2	2	2	1	2	2
29	2	2	2	2	2	2	2	2	1	2	2	2	2	2	2
30	1	2	2	2	2	2	2	2	1	2	2	2	2	2	1
31	1	1	2	2	2	2	2	2	2	1	2	2	2	1	1
32	2	1	2	2	2	2	2	2	1	2	2	2	2	1	1
33	2	1	1	2	2	2	2	1	2	2	2	2	1	1	1
34	2	2	1	1	2	2	2	2	2	2	2	2	1	2	1
35	1	2	2	1	2	2	2	2	2	2	2	1	1	1	1
36	2	1	2	1	1	2	2	2	2	2	1	1	1	1	2
37	1	1	2	2	1	1	2	2	2	1	1	1	1	1	1
38	1	1	2	1	1	2	2	2	1	2	1	1	1	2	1

Fig. 5. Results of the F-test (10%).

LINE \ COLUMN	216	217	218	219	220	221	222	223	224	225	226	227	228	229	230
24	209	216	217	219	218	216	217	213	185	71	82	79	84	85	88
25	206	212	216	218	217	218	214	219	206	91	91	82	83	87	87
26	195	208	213	216	219	219	218	221	218	193	78	89	85	87	78
27	126	203	210	215	218	221	220	218	221	214	104	104	89	80	86
28	108	191	207	214	219	220	218	220	217	221	210	89	90	83	20
29	116	116	200	213	217	219	221	221	221	215	220	197	29	20	24
30	110	106	183	210	215	218	221	223	223	221	225	215	19	29	17
31	109	114	110	196	209	216	219	223	225	222	206	220	15	20	15
32	110	112	123	127	204	214	219	224	223	217	184	218	43	17	14
33	112	113	117	111	186	212	221	218	216	192	224	14	27	15	16
34	114	114	116	122	117	208	220	210	191	221	20	36	19	16	17
35	116	117	118	121	132	139	187	181	214	23	40	22	18	18	18
36	117	118	120	122	129	144	153	194	24	41	24	18	19	19	19
37	118	119	116	124	126	123	159	25	38	23	19	18	18	18	20
38	119	121	119	124	119	125	30	35	22	19	18	17	17	18	21

Fig. 6. Enhanced image (level of significance 1%).

LINE \ COLUMN	216	217	218	219	220	221	222	223	224	225	226	227	228	229	230
24	209	216	217	219	218	219	217	213	185	71	82	79	84	81	88
25	206	212	216	218	219	218	222	219	206	91	74	82	88	87	87
26	195	208	213	216	219	221	218	221	218	193	78	89	91	87	94
27	126	203	210	215	218	221	220	223	221	214	104	80	89	92	86
28	108	191	207	214	219	220	218	220	223	221	210	89	90	83	20
29	107	116	200	213	217	219	221	223	221	223	220	197	29	20	14
30	110	106	183	210	215	218	221	223	223	226	225	215	19	9	17
31	109	114	110	196	209	216	219	223	225	222	226	220	15	20	15
32	112	112	107	127	204	214	219	224	223	226	225	218	9	17	14
33	109	113	117	111	186	212	221	218	225	224	224	14	27	15	16
34	112	119	116	122	117	208	220	223	222	221	20	12	19	19	17
35	116	114	122	121	115	139	214	217	214	23	16	22	18	18	18
36	119	118	124	122	129	123	199	194	24	17	24	18	19	19	17
37	118	119	116	126	126	123	159	25	18	23	19	18	18	18	20
38	119	121	119	124	119	125	30	18	22	17	18	17	17	14	21

Fig. 7. Enhanced image (level of significance 10%).

tion region. Then, an increased number of neighborhoods are assumed to contain an edge.

Figures 6 and 7 show the resulting enhanced numerical images for levels of significance of 1% and 10%, respectively.

Tables 1 and 2 present the performance of the proposed algorithm when applied to the Lenna image [Fig. 1(a)] in terms of the percentile of pixels altered at each iteration (NPI) and also in terms of total changes introduced at each iteration, measured in digital numbers (RDC):

$$\mathrm{RDC} = \frac{\sum_1^N [\mathrm{DN(new)} - \mathrm{DN(old)}]}{N},$$

with N being the total number of pixels processed.

It can be seen that the number of pixels that have the digital number altered (NPI) decreases after each iteration.

RDC measures the intensity of the changes in terms of digital number values after each iteration. The highest values for RDC occur at the initial iterations and RDC decreases rapidly.

The effect of the level of significance for the F-test can also be observed here. For a level of significance of 10%, RDC decreases faster than for 1%. The same relation can be observed for NPI. As higher values of significance increase the rejection region and cause more neighborhoods to be treated as a probable edge, the contrast in the image is increased and, therefore, more changes are introduced at each iteration. On the other hand, lower values for the level of significance lead to a larger number of homogeneous regions, as shown in Figs 4 and 5. This causes a smoothing effect on the image and, therefore, a stable situation is reached earlier.

Table 1. Values of RDC and NPI for Lenna image (level of significance of 1%)

Iteration	RDC	Delta (RDC)	NPI%	Delta (NPI)
1	5.4469		88.6276	
2	3.9810	−1.4570	78.3432	−10.2844
3	3.3496	−0.6403	76.7517	−1.5915
4	3.1316	−0.2180	73.6267	−3.1250
5	2.9140	−0.2170	72.0398	−1.5869
6	2.8022	−0.1118	70.5643	−1.4755
7	2.6825	−0.1197	69.8990	−0.6653
8	2.5911	−0.0914	68.3853	−1.5137
9	2.5304	−0.0608	68.0267	−0.3586
10	2.4540	−0.0764	67.2882	−0.7385
11	2.4050	−0.0489	66.1041	−1.1841
12	2.3527	−0.0523	65.7944	−0.3097
13	2.3106	−0.0421	64.9582	−0.8362
14	2.2683	−0.0423	64.1418	−0.8164
15	2.2535	−0.0147	63.9252	−0.2166
16	2.2166	−0.0369	63.1790	−0.7462
17	2.1709	−0.0458	62.8601	−0.3189
18	2.1449	−0.0259	62.4542	−0.4059
19	2.1202	−0.0247	61.7447	−0.7095
20	2.0989	−0.0213	61.3831	−0.3616

Table 2. Values of RDC and NPI for the Lenna image (level of significance of 10%)

Iteration	RDC	Delta (RDC)	NPI%	Delta (NPI%)
1	5.3416		88.0173	
2	3.7649	−1.5767	76.7210	−11.2963
3	2.9468	−0.8181	68.7210	−8.0000
4	2.4868	−0.4600	64.0778	−4.6432
5	2.2910	−0.1958	60.7178	−3.3600
6	2.1505	−0.1404	57.4966	−3.2212
7	2.1030	−0.0475	55.1880	−2.3086
8	2.0403	−0.0627	54.0375	−1.1505
9	1.9467	−0.0937	52.8946	−1.1429
10	1.8588	−0.0879	51.6815	−1.2131
11	1.8029	−0.0559	50.6073	−1.0742
12	1.7658	−0.0371	49.3958	−1.2115
13	1.7282	−0.0376	48.6298	−0.7660
14	1.6720	−0.0561	47.8897	−0.7401
15	1.6528	−0.0193	47.1085	−0.7812
16	1.6317	−0.0211	46.8536	−0.2549
17	1.6062	−0.0254	46.2997	−0.5539
18	1.5722	−0.0340	45.9152	−0.3845
19	1.5287	−0.0435	45.1355	−0.7797
20	1.5051	−0.0237	44.6701	−0.4654

4. CONCLUSIONS

An adaptive filtering approach for image enhancement is presented in this paper. The algorithm first detects borders between radiometrically distinct regions and then applies a weighting function to smooth internally the more or less homogeneous regions or image classes and, at the same time, sharpens the borders between them. Smoothing is performed when the region is considered to be homogeneous and enhancement is performed when a probable edge is found.

Edges in an image are often not easily detected, especially when one is dealing with small neighborhoods, but the F-test applied to identify probable edges worked efficiently, providing the conditions to perform selective filtering.

The use of a weighting factor in computing new digital numbers makes it possible to control these changes as a function of the values within the neighborhood of each pixel, reducing probable errors at points where the F-test could deliver ambiguous results.

It was proved that both concepts perform efficiently, allowing the proposed algorithm to be effective when applied to real images, improving the spatial definition of the objects present, and allowing for better conditions to its identification.

Acknowledgements—The authors would like to thank the Institut für Photogrammetrie und Fernerkundung IPF, Universität Karlsruhe and the Remote Sensing Center, Federal University at Rio Grande do Sul, Brazil, for the support that made this study possible. Image Lenna was obtained from ftp://teleos.com/VISION-LIST-ARCHIVE/IMAGERY.

REFERENCES

1. R. C. Gonzalez and R. E. Wood, *Digital Image Processing*, Chapter 4. Addison-Wesley, Reading, Menlo Park, New York (1993).
2. A. Rosenfeld and A. C. Kak, *Digital Picture Processing*, Vol. 1, Chapter 6. Academic Press, New York (1982).
3. R. M. Haralick, Edge and region analysis for digital image data, *Image Modeling*, A. Rosenfeld, ed., pp. 171–184. Academic Press, New York (1981).
4. H.P. Kramer and J.B. Bruckner, Iterations of a non-linear transformation for enhancement of digital images, *Pattern Recognition* **1**, 53–58 (1975).
5. S. K. Pal and M. D. Dutta Mahunder, *Fuzzy Mathematical Approach to Pattern Recognition*, Chapter 12. Wiley, New York (1986).

About the Author—JORGE ANTONIO SILVA CENTENO was born in La Paz, Bolivia. He received the Diploma in Civil Engineering from the Federal University of Mato Grosso, Brazil, in 1984 and the M.Sc. degree from the Federal University of Rio Grande do Sul, Brazil. He worked as a researcher for CNPq/Brazil at the State Center for Meteorology and Water Resources in the State of Alagoas, Brazil. Currently he is a Ph.D. candidate at the Institute for Photogrammetry and Remote Sensing, University of Karlsruhe, Karlsruhe, Germany.

About the Author—VICTOR HAERTEL was born in Porto Alegre, Brazil. He received the diploma in Civil Engineering from the Federal University of Rio Grande do Sul, Brazil; the M.Sc. degree from the International Institute for Aerospace Survey and Earth Sciences (ITC), The Netherlands and the Ph.D. degree from Colorado State University. Dr Haertel is currently an Associate Professor of Remote Sensing and Director of the Remote Sensing Center, Federal University of Rio Grande do Sul, Brazil. His research interests include methods for digital image processing and classification in remote sensing.